Development 130, 873-887

doi:10.1242/dev.00314

Shaping the zebrafish notochord

Nathalia S. Glickman[1,*], Charles B. Kimmel[1], Martha A. Jones[1] and Richard J. Adams[2,†,‡]

[1]Institute of Neuroscience, University of Oregon, Eugene, OR 97403-1254, USA
[2]Department of Biology and Biochemistry, University of Bath, Bath BA2 7AY, UK

*Present address: Developmental Genetics Program and Department of Cell Biology, Skirball Institute of Biomolecular Medicine, New York University School of Medicine, New York, NY 10016, USA
†Present address: Department of Anatomy, University of Cambridge, Downing Street, Cambridge CB2 3DY, UK
‡Author for correspondence (e-mail: rja46@cam.ac.uk)

Accepted 18 November 2002

SUMMARY

Promptly after the notochord domain is specified in the vertebrate dorsal mesoderm, it undergoes dramatic morphogenesis. Beginning during gastrulation, convergence and extension movements change a squat cellular array into a narrow, elongated one that defines the primary axis of the embryo. Convergence and extension might be coupled by a highly organized cellular intermixing known as mediolateral intercalation behavior (MIB). To learn whether MIB drives early morphogenesis of the zebrafish notochord, we made 4D recordings and quantitatively analyzed both local cellular interactions and global changes in the shape of the dorsal mesodermal field. We show that MIB appears to mediate convergence and can account for extension throughout the dorsal mesoderm. Comparing the notochord and adjacent somitic mesoderm reveals that extension can be regulated separately from convergence. Moreover, mutational analysis shows that extension does not require convergence. Hence, a cellular machine separate from MIB that can drive dorsal mesodermal extension exists in the zebrafish gastrula. The likely redundant control of morphogenesis may provide for plasticity at this critical stage of early development.

Movies available on-line

Key words: Gradients, Morphogenesis, *no tail*, Mediolateral intercalation behavior, Notochord, Convergence, Extension, Gastrulation, Epiboly, Zebrafish

INTRODUCTION

Cellular reorganization based on active cell motility and adhesion is the major means of morphogenesis in animal embryos, and is particularly elaborated in vertebrates. Nowhere is this fact more clearly shown than in the dorsal mesoderm of gastrulating zebrafish embryos. Here, occurring in the company of both cellular internalization at the blastoderm margin (Carmany-Rampey and Schier, 2001) (R. J. A., D. Faruque and M. L. Concha, unpublished) to form the mesoderm and an equally prominent spreading of the blastoderm by epiboly (Warga and Kimmel, 1990), there is a rapid and massive cellular reorganization. The reorganization underlies mesodermal convergence, meaning the narrowing of the tissue with respect to the embryonic axis (the anteroposterior, or AP axis), and mesodermal extension – the lengthening of the tissue with respect this axis.

Our current view of the cellular behaviors that drive these tissue-level shape changes comes primarily from a series of studies of explanted *Xenopus* dorsal mesoderm (Shih and Keller, 1992a; Shih and Keller, 1992b; Keller et al., 2000). Molecular and genetic studies (including studies in zebrafish and other species) have enriched our current understanding (Solnica-Krezel, 1999; Tada and Concha, 2001; Wallingford and Harland, 2001; Myers et al., 2002a; Myers et al., 2002b). The explant studies in *Xenopus* show that dorsal mesodermal converges and extends largely by cell rearrangement within the tissue, and without dependence upon an external substrate (Shih and Keller, 1992a). Furthermore, from this work has evolved the concept of a single but complex cellular behavior, termed mediolateral intercalation behavior (MIB), which underlies the rearrangements (Fig. 1). The MIB hypothesis is elegant because a single force-generating cellular machine, distributed across a field of cells, produces both convergence and extension, both narrowing and elongation of the field. By the MIB hypothesis, as applied particularly to the domain of notochord-forming cells within dorsal mesoderm, motile and adhesive cells become polarized along one particular axis, the mediolateral (ML) axis. The polarity may depend on, and be coordinated within the field, by a noncanonical Wnt signaling planar polarity pathway (Choi and Han, 2002; Heisenberg et al., 2000). The cells take on a bipolar shape, elongating along the ML axis. This process requires that the individual cells all correctly orient actin-based cytoskeletal machinery that mediates motility, and perhaps also orient associated adhesion complexes on their plasma membranes (Montell, 1999; Zalik et al., 1999). Localized release of intracellular Ca^{2+}, via connexin 43 channels (Essner et al., 1996), and activation of Rho GTPases may be crucial in such polarized cellular morphogenesis (Choi and Han, 2002; Hall and Nobes, 2000; Smith et al., 2000). The cells intercalate mediolaterally. To accomplish this, they all protrude filopodial processes both

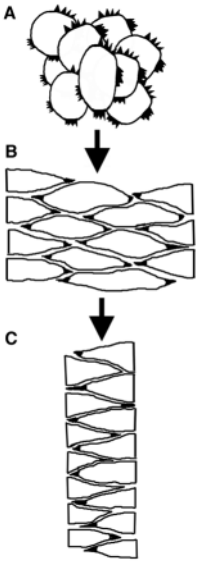

Fig. 1. The mediolateral intercalation behavior (MIB) hypothesis. (A) Early protrusive activity is random. (B) The cells take on a bipolar shape as their protrusions are restricted to the ML axis. Protrusive activity is not present at the notochord/somite boundaries (to the sides). (C) The field narrows and elongates (converges and extends) as the cells exert traction upon one another and pull together. Adapted, with permission, from Shih and Keller (Shih and Keller, 1992a).

medially and laterally that extend between immediate cellular neighbors, and new cell-cell contacts are made, perhaps involving adhesion molecules of the cadherin/protocadherin superfamily localized to their filopodial tips (Keller et al., 2000). The newly contacting cells then contract their processes. They exert traction upon one another and pull together. Such events, which occur across the entire field of cells, narrow the field (convergence). The resulting intercalations push previously neighboring cells apart along the AP axis, lengthening the field along this axis (extension).

Previous work suggests that MIB may also underlie convergence and extension in the zebrafish gastrula (Concha and Adams, 1998; Heisenberg et al., 2000; Kimmel et al., 1994; Solnica-Krezel et al., 1996; Warga and Kimmel, 1990; Myers et al., 2002a; Myers et al., 2002b). The cells disperse along the AP axis by intercalating with neighbors to form a discontinuous AP string, as expected if MIB mediates extension (Kimmel and Warga, 1986; Kimmel et al., 1994). However, it is not known to what extent the phenomenon is coupled to convergence as the MIB hypothesis predicts it should be. Additionally, other more coherent cellular flows, e.g. migrations that do not involve cellular intercalations, might also occur to increase the AP length of the developing notochord.

To test the MIB model in zebrafish, we used a confocal microscope to image and make time-lapse recordings of the dorsal mesoderm in dye-labeled intact wild-type (WT) and *no tail* (*ntl*) mutant embryos (Cooper et al., 1999b) (N. S. Glickman, PhD Thesis, University of Oregon, 2000). *ntl* is the zebrafish homolog of the mouse T-box gene *Brachyury* (Schulte-Merker et al., 1994). Our recordings begin during gastrulation, shortly after mesodermal internalization at the blastoderm margin, and we followed the movements of most of the cells in the field of view during convergence and extension. The method differs significantly from most previous studies in that confocal imaging, 4D recording and cell-by-cell analysis of these records allows us to keep track of, and quantify, the behaviors (e.g. movement velocities and intercalation behaviors) of a substantial fraction of the dorsal mesodermal cells rather than just a small sample. We use this method to measure rate constants for convergence and extension, providing for meaningful comparison between tissues or embryos.

We find that the rate of convergence within the notochord domain is comparable with that in the somite, whereas extension is several-fold higher in the notochord than in the somite, suggesting that the cells are reorganizing differently in the two domains. Quantitative features of convergence and extension and local cellular reorganizations within notochord domain are as expected from the MIB hypothesis. Our data suggest furthermore that for the WT notochord domain, MIB quantitatively accounts for the observed morphogenesis. We show that *ntl* is a key regulator of convergence of the notochord domain; in *ntl* mutants, convergence is severely disrupted, and our analyses suggest that MIB is initiated but cannot be completed. Surprisingly, in the near absence of early convergence in *ntl* mutants, the dorsal mesoderm can still extend. Hence, extension does not require MIB. We discuss the meaning of these finding for understanding mesodermal morphogenesis and its regulation.

MATERIALS AND METHODS

Fish stocks

Adult zebrafish (*Danio rerio*) and embryos were reared at 28.5°C, as described by Westerfield (Westerfield, 1995), and staged in accordance with Kimmel et al. (Kimmel et al., 1995). We performed time-lapse recordings with wild-type (strain AB) embryos and with the mutant and wild-type siblings of *ntl*^{b195} (Halpern et al., 1993). The *ntl*^{b195} allele is caused by an insertion, resulting in a stop codon and a truncated non-functional protein (Schulte-Merker et al., 1994).

Time-lapse production and analysis

Dechorionated embryos (3.3-3.5 hpf) (Kimmel et al., 1995) were incubated in embryo rearing medium plus 10 mM HEPES buffer (pH 7.2) (Cooper et al., 1999a; Cooper et al., 1999b; Westerfield, 1995). Embryos were stained in 100 μM BODIPY FL C5-Cer/C5-DMB-Cer (N-(4,4-difluoro-5,7-dimethyl-4-bora-3a,4a-diaza-s-indacene-3-pentanoyl) sphingosine (in 1% DMSO), here after referred to as BODIPY ceramide (Molecular Probes) (Cooper et al., 1999a; Cooper et al., 1999b).

Embryos were mounted in a viewing chamber (Westerfield, 1995) in 3% methylcellulose and 0.3% agar, dorsal side upwards. We examined seven wild-type embryos and four *ntl* mutant embryos. Images were taken with a Zeiss 310 upright confocal microscope with a Kr/Ar laser. We imaged 12 focal planes, at 3 μm intervals for each time point, set 2 minutes apart. The 4D confocal images were compiled into a 4D movie for playing in a modified version of NIH image. Cell locations over time were collected using a modified version of NIH Image (Wasband, NIH) customized to animate 3D time-lapse image series. Each cell was traced over time by manually marking its approximate geometric center in three dimensions through each time frame, recording all cell divisions and final cell fate from its location. All data produced in this way were further analyzed by routines written in the analysis environment IDL (Research Systems Inc, CO). Final presentations were rendered by code generated for the ray-tracer POVRay (POVray).

The precise records of cell positions over time allow us to generate metrics that describe the patterns of motion of morphogenesis. The raw cell tracks were rotated in space to align the AP axis vertically. AP location and velocities can then be expressed in terms of y coordinate and velocities calculated as $\mathrm{d}y/\mathrm{d}t$. Similarly, mediolateral movements proceed in x with velocities of $\mathrm{d}x/\mathrm{d}t$. Cell velocity and speed were calculated as changes in location about the time frame of interest e.g. $\mathrm{d}x/\mathrm{d}t$ at time t is calculated from the displacement $x[t+\mathrm{I}]$

– $x[t\text{-I}]$ for a short period I, usually ±8 minutes. The area of the entire tracked field and the tracked axial domain was measured by drawing a convex hull around all the tracked cells. The width of the field of tracked cells is the mean width of the lateral edges of the hull. The 2D density of the tracked field was approximated by dividing the area contained by the convex hull by the number of cells within the box. This measure is approximate and assumes cells are uniformly tracked through time, to reduce possible errors the relative change in density rather than absolute measures were used in these analyses.

In order to analyze average local cell rearrangement, we calculated for each cell in turn the relative location and movement of each other cell in its vicinity. Then a smoothed map of all accumulated relative cell movements was used to generate a vector field to visualize the mean local tissue shape change during a short epoch.

Specific cell rearrangement motifs can be looked for in the cell tracks by calculating a connectivity matrix that describes adjacency of neighboring cells based upon their geometry in space (2D or 3D). Neighbor changes will reflect, for example, intercalation events because as two cells move towards each other mediolaterally, they become new neighbors and displace their anterior and posterior neighbors. The analysis of neighbor changes are limited to the wild-type and mutant notochord/axial domains, where the optics are best and we have most completely tracked the cell populations. We calculated the immediate cell neighbors of all traced cells for each time frame, from a complete 3D Delaunay triangulation. The program Qhull (Barber et al., 1996) was built as a library callable from within IDL for this purpose. Each vertex corresponds to the location of a cell. The algorithm assumes that the local field has been completely tracked, that cells are compact in shape and are in close contact with their neighbors – as is evident from inspection of the field (see below, Fig. 3A). To exclude erroneous apparent neighbor changes between non-contiguous cells, a conservative maximum cell spacing of 18 μm was used. Any cells separated by an edge longer than this threshold were not considered to be neighbors for this analysis. (In practice, the patterns of change seen in connections were relatively insensitive to variation in this threshold, despite significant changes in the total number of permitted connections.) Changes in neighbor connections over time were detected from the changes in connectivity in the triangulation. Changes due to cell divisions, cells moving into and out of the traced field, and transient make-break events were excluded from the analysis. Hand-checking a set of such identified intercalations, in the original 4D record set, showed the accuracy of the computer-assisted method to be at least 90%. The angle at which cells make and break connections reflects the angle of the interaction event. The distributions of angles were tested for uniformity using a Watson U^2 test and any samples found to be non-random ($P<0.05$) were tested for their mean axial alignment. Variations in alignment over time were visualized by a moving sample window through the duration of the experiment.

Calculating the convergence and extension rate constants

The position dependence of the rate of cell movement (dx/dt) is apparent when the rate of ML cell movement is plotted against its ML position (x). A linear variation of velocity with location is related by a rate constant, equivalent to a first-order kinetic constant, $dx/dt=kx$. A linear slope, calculated by regression of this plot, is known as the convergence rate constant k_c. For an unchanging constant this would cause any individual cell to describe an exponential path of location over time $x_t=x_0.e^{k.t}$. In practice, the rate constant k_c varies over time by some small range giving

$$x_t = x_0 e^{\int_0^t k_t}.$$

For the purposes of comparison between experiments, an equivalent single rate constant equal to the mean rate over that interval can be used. The same calculations were made for an extension rate constant k_E, but in this case, the change in the AP position (dy/dt) of each cell was calculated.

We made a simulation to show how an idealized 2D field of cells would reorganize if converging with a linear velocity gradient in space and extending with an equal gradient of opposite sign (thus preserving cell density), see Fig. 2. A hexagonal array of cells was incrementally constricted and stretched to demonstrate the resulting affect. Globally, the field narrowed exponentially and extended exponentially, as expected. Individual cell reorganization relative to adjacent neighbors was constant and reiterated across the field.

RESULTS

Predicted features of mediolateral intercalation behavior (MIB)

In the simplest version of the MIB hypothesis, cells pull together by intercalation along the mediolateral (ML) axis and simultaneously are pushed apart along the AP axis. The hypothesis makes a number of verifiable predictions, illustrated by an animation of hypothetical ‘cells’ undergoing MIB (Fig. 2A-D; movies for this and other figures are available as supplemental information at http://dev.biologists.org/supplemental/). During the sequence illustrated, the field of cells narrows to half of its original width (convergence – along the horizontal in Fig. 2), and elongates to twice its original length (extension – along the vertical). The amount of narrowing equals the amount of lengthening, i.e. convergence equals extension.

During MIB cells reorganize, as illustrated by close-up views near the field center (*) at the beginning (Fig. 2E) and end (Fig. 2F) of the same sequence. A single cell (*) retains several of its original neighbors (numbered for identification) but changes others. Cells that start out a rank apart along the ML axis become new neighbors (e.g. cells 2 and 6). Conversely, cells that were neighbors along the AP axis become separated by a rank (e.g. cells 1 and 10). This local reorganization is uniform across the field.

Strikingly, however, movement velocities of the cells are not uniform because of the incremental nature of MIB. The cell at the center (*; which we shall see represents a point along the midline of the embryo) does not move. Cell 8 moves inward a single rank, and cell 9, located three times as far away along the ML axis, moves inward three ranks (Fig. 2E,F), moving three times faster because it is pulled by its own intercalations and also pulled by inward-moving more medial cells. ‘Converging’ cells move inwards with a velocity proportional to their distance from the midline, such that a linear gradient of velocity with position is present across the field (Fig. 2H). This position dependence on the rate of movement can also be seen by examining the paths the cells take during a given time interval (Fig. 2G). The paths of the cells at more lateral positions are longer than the paths of cells close to the center, reflecting their rate of travel.

Similarly, along the AP axis the rate of outwards movement depends on AP position. Cell 11 is three times farther from the center than cell #1 and it moves three times faster (Fig. 2E,F). Again, the relationship between cellular position in the field and velocity is linear (Fig. 2I). The slopes of the lines in Fig. 2H,I give convenient measures (rate constants) for convergence and extension (k_c and k_E, respectively). The convergence rate

constant is negative, reflecting inward movement, and the extension rate constant is positive, reflecting outward movement. Their absolute values are equal.

The MIB hypothesis thus predicts linear gradients of velocity with position. Furthermore, it follows from the same arguments that the shape changes of the field should not be constant with time. As the field narrows during convergence, only smaller ML positional values remain (the larger ones are lost as the population moves closer the midline) and only lower velocities should be observed. Hence, the rate of change in field width should decrease with time. As the field lengthens during extension new, larger AP positional values are established and velocities are correspondingly higher. Hence, the rate of change in field length should increase with time. The kinetics are exponential in both cases (Fig. 2J,I), and the exponential curves have the same slopes as the gradients described above: k_C and k_E.

A perhaps surprising feature of MIB is that a large change in shape of the cellular field is produced by relatively small local cellular rearrangements. This is another prediction of the hypothesis.

Tissue domains and cellular flows

Convergence and extension in embryos has usually been measured by tracking the movements of one or more labeled cells or small cell groups toward the dorsal midline, and along the AP axis. The above analyses show clearly that this method is unreliable when used to make interpretations about the movement of the entire field of cells. Even where convergence and extension are uniform across the field and during time, the ML and AP cellular velocities are not uniform with time, and depend on cell position within the field. Hence, we used a labeling and recording method (Cooper et al., 1999a; Cooper et al., 1999b), and analytical tools (Concha and Adams, 1998) (see Materials and Methods) that allowed us to keep track of all or most of the cells being recorded, and we tracked the field of developing cells as fully as we could. Fig. 3 illustrates the results for a wild-type embryo. Cell outlines are apparent in the time series of original recordings (A), and the series of records with respect to both time and depth (*z*-axis sectioning with the confocal microscope) intervals were close enough to one another to permit us to follow unambiguously individual cells in the field of view, no matter how the cells moved, and during cell divisions. The field is approximately centered on the dorsal midline, and the particular *z*-level illustrated in Fig. 3A is at an intermediate depth through the internalized prospective mesoderm (or hypoblast) at the center of the field. The blastoderm margin is evident at first (Fig. 3A1), and then, because of epiboly (Kimmel et al., 1995; Solnica-Krezel et al., 1996), it moves off towards the vegetal pole (downwards in the figure), out of the field being recorded. Brachet's cleft (Kimmel et al., 1995), the boundary between ectoderm and mesoderm, is evident (arrows in Fig. 3A2).

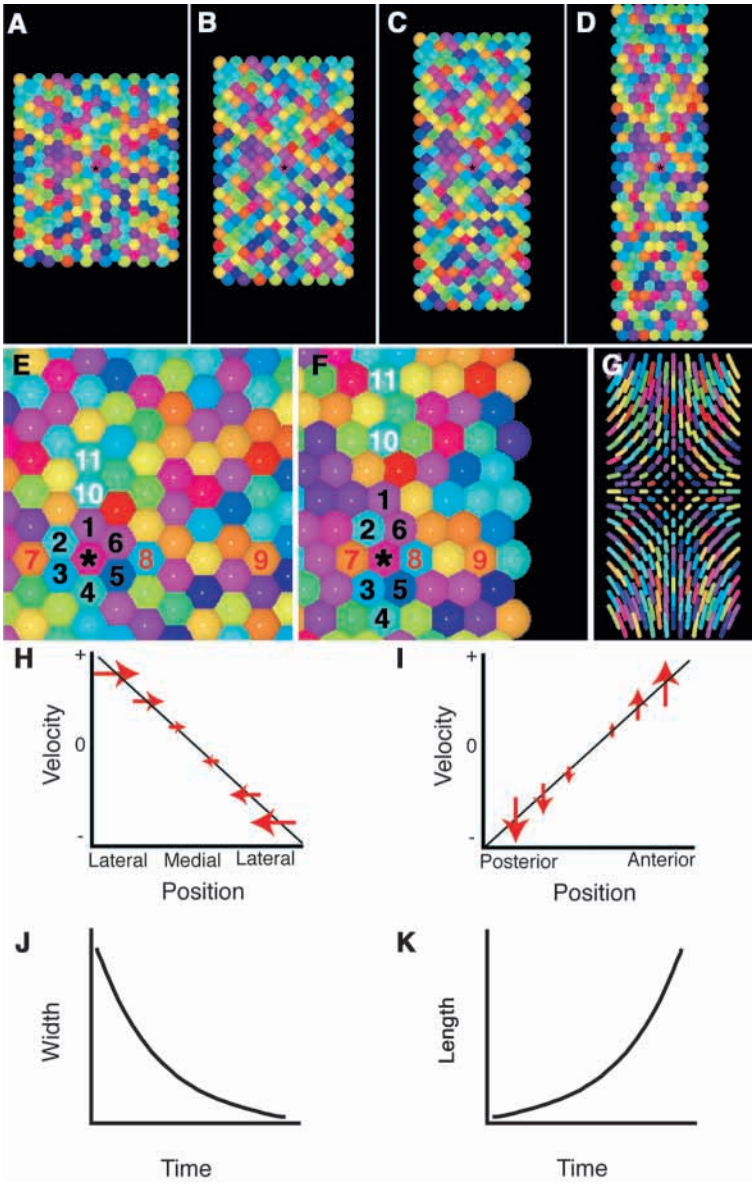

Fig. 2. Predicted rearrangements and movement kinetics in a field of hypothetical 'cells' uniformly expressing MIB (see Movie 1 at http://dev.biologists.org/supplemental/). (A-D) Time course of rearrangements of the cells (spheres) undergoing convergence and extension. The field halves in width and doubles in length over the period of A to D; the intermediate stages (B,C) represent the field at one- and two-thirds of completion of the round of MIB. The area and thickness of the field does not change, and MIB is constant with respect to cell position and time. (E,F) Close-up views near the field center (*) at the beginning (E) and end (F) of the same sequence. See the text for description of the local cellular reorganizations. (G) The cellular flows resulting from intercalations occurring between times B and C. The most rapidly moving cells (longest lines) are those most distant from the center. (H,I) Linear gradients relate ML velocity with ML position (H, convergence) and AP velocity with AP position (I, extension). The red arrows indicate the directions and rates of cell movement (ML movement is inwards, AP movement is outwards) such that the gradient slopes are opposite in sign. (J,K) The field width decreases exponentially (J), and the field length increases exponentially (K). Cell position at a given time *t* can be predicted by the relationships $x_t=x_0e^{k_ct}$ and $y_t=y_0e^{k_et}$.

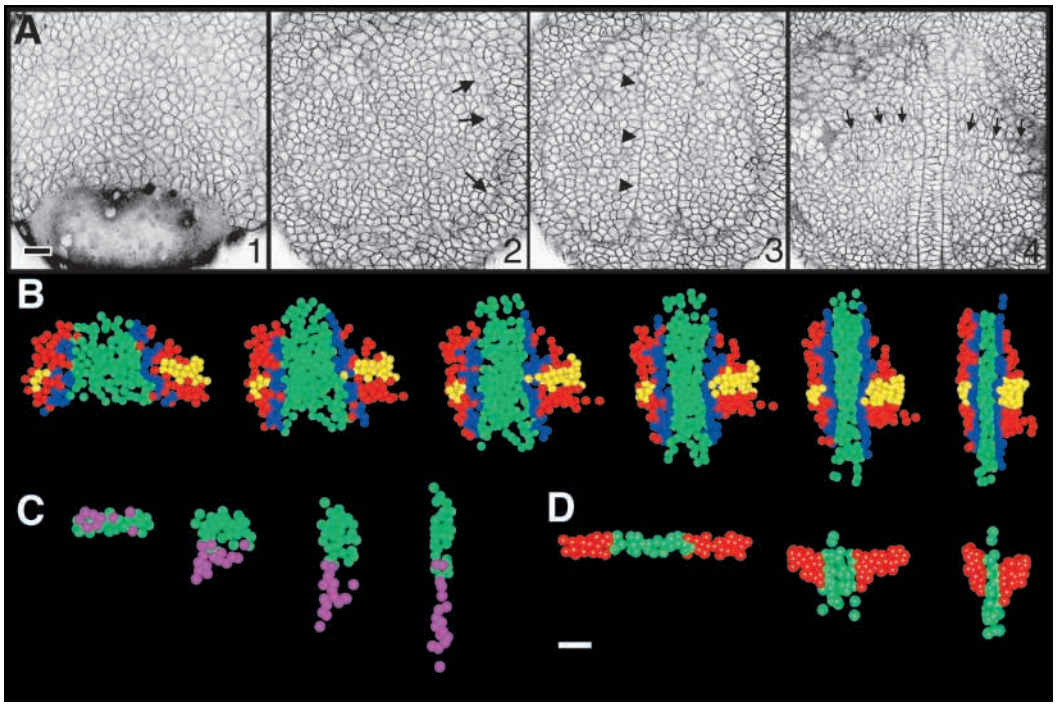

Fig. 3. Convergence and extension of zebrafish dorsal mesoderm. Time sequences taken from a single 4-hour 4D recording of a wild-type embryo, beginning at midgastrula stage (7.3 hpf) (Kimmel et al., 1995) (see Movies 2-5 at http://dev.biologists.org/supplemental/). The AP axis is vertical (anterior towards the top), and the ML axis horizontal, here and in Figs 5-7, Fig. 9, Fig. 11. The field is centered approximately on the dorsal midline. (A) Views from the recording, at 7.3 (A1), 8.8 (A2), 9.3 (A3) and 11.3 (A4) hpf (hours postfertilization). Negative confocal microscope images of the BODIPY-ceramide labeled cellular field are shown. At the first time point (A1) the blastoderm margin is evident, separating the cellular blastoderm (upper) from the yolk syncytial layer (YSL, lower). Subsequently, the blastoderm comes to cover the yolk completely by the spreading movement of epiboly. Brachet's cleft, which appears as a hazy ring (arrows, A2), separates ectoderm to the outside, and mesoderm to the inside. The notochord/somite boundaries (axial/paraxial boundaries: arrowheads, A3) appear in the mesoderm. They are barely visible in A2 and then become prominent. Convergence narrows the notochord domain to about 2 cells wide at the last time point (A4). At the lateral side of each boundary lies a distinctive row of somitic adaxial cells that will form slow muscle (Blagden et al., 1997; Devoto et al., 1996). In addition, the somite boundaries are visible and are marked by arrows. (B) About 200 cells, represented as spheres, were tracked from the recording and are shown at 7.3, 8.3, 8.8, 9.3, 10.3 and 11.3 hpf. Cells are color-coded according to their eventual fates: notochord-forming cells (green), adaxial cells (dark blue), cells that form somite 2 (yellow) and other somite-domain cells (red). Nearly all of the cells divided during course of the 4 hour recording. Almost without exception, both siblings ended up in the same domain, and we color-coded the mother cell identically to its daughters. The notochord, and somite domains are spatially separate from the outset of the recording, even though distinctive boundaries are not yet present (A1). (C) Notochord-forming cells (green) and overlying floorplate-forming cells (magenta) shear relative to one and other during extension (48 floor plate-forming cells were tracked). The two cell types were collected from separate focal planes of the original 4D recording, and a 30 μm stripe cut at a single AP level is shown at 7.3, 8.3, 9.3 and 11.3 hpf. (D) The notochord domain (green) extends more than the somite domains (red). A 30 μm horizontal stripe of mesoderm cut from the field and is shown at 7.3, 9.3 and 11.3 hpf. Scale bar: 50 μm.

Animating a recording such as used for Fig. 3A (see Movie 2 at http://dev.biologists.org/supplemental/) reveals that the overall cellular flows are as expected of MIB (Fig. 2G). Movement pathways of lateral cells are predominantly ML, whereas those of medial cells are predominantly AP (see Myers et al., 2002b). The animation also allows visualization of another predicted feature of MIB: the position-dependent rates of cell movement (Fig. 2H,I). Lateral cells move towards the midline faster than cells already close to the midline. Cells near the top and bottom of the field move faster along the AP axis than those near the middle of the field.

Within the mesoderm at 9.3 hpf, boundaries between the prospective notochord and presomitic mesoderm become clearly visible (notochord-somite or axial-paraxial boundaries; arrowheads, Fig. 3A3). By animating the recordings, and playing Movies 2 and 3 backwards (see http://dev.biologists.org/supplemental/), one can see that these boundaries arise in a patchy (or piecemeal) way; they can be vaguely recognized in Fig. 3A2 (8.8 hpf), farther apart than at later stages, thus revealing that the notochord domain is converging. However, the boundaries are not at all visible at the initial time point (7.3 hpf, midgastrula period). At the last time point, 4 hours later, the notochord-somite boundaries have straightened out and come together to enclose a notochord domain that is now only two or three cells wide (Fig. 3A4). The boundaries between the most anterior somites are also just becoming visible (arrows, Fig. 3A4).

Once such landmarks become visible, we could assign cells particular fates (e.g. position of a cell within the area demarcated by the notochord boundaries defines a notochord cell). Fig. 3B shows a time series from the same records, where we represent tracked cells as spheres color-coded according to these eventual fates. We find, in this and in other wild-type embryos similarly analyzed, that the notochord domain is coherent from outset of the recording; i.e. the domain of prospective notochord cells is spatially separate from the somitic domains (and also from overlying floorplate-forming cells, Fig. 3C), before overt boundaries arise. During convergence, the notochord domain narrows from 10-14 cells across at the time our recording begins to two or three cells across. This kind of decrease is expected from sustained MIB.

Differential movements can be detected between regions adopting different fates. For example, we observe slipping

apart or shear between cells the notochord domain and the immediately overlying floor plate-forming cells in the prospective neural plate. As is evident in Fig. 3C, the notochord and floor plate-forming cells start out at the same AP position but after undergoing marked convergence and extension, the final position of the floor plate-forming cells is posterior relative to the notochord cells. Tracking other cells in the epiblast (i.e. in the prospective neural plate outside of the medial floor plate domain; data not shown) reveals that this shearing is not unique to the notochord and floorplate, but is a general feature of epiblast cellular movement relative to that in the internalized mesoderm of the hypoblast. We can account for the shear by considering the combined morphogenetic movements of epiboly and internalization of cells by ingression at the blastoderm margin (see Discussion).

The notochord domain also shears with the neighboring somite domains (Fig. 3D), as previously reported at later stages in zebrafish by Devoto et al. (Devoto et al., 1996). In this case, as we describe next, we can account for the shearing by a difference in the rate in which the two domains extend. The presentation in Fig. 3D reveals that extension of the notochord domain is dramatically greater than extension of the somite mesoderm. The same difference is also present in *Xenopus* (Keller et al., 1989; Keller et al., 2000).

Rates of convergence and extension

We quantitatively analyzed the kinetics of the cellular flows in our records to explore further the similarities and differences in convergence and extension in the notochord and somite domains. We observed that during gastrulation and continuing into the early segmentation period of development, the width of the notochord domain decreases with the kinetics of exponential decay (Fig. 4A), as predicted by the MIB hypothesis (Fig. 2J). This finding suggests that if MIB, or a similar mechanism underlies convergence, cellular interactions (including rates of ML intercalations) remain approximately constant during the recording period.

Plotting ML velocities of all the cells tracked in the field as a function of their ML position, at any time point, reveals the linear gradient underlying convergence (Fig. 4B) predicted by the model (Fig. 2H). As shown in Fig. 4B, the data points for the velocities of cells in left and right somite domains (red) fall on the same line as those for cells in the notochord domain (green). This finding shows that the rates of convergence in the three domains are similar. Calculating the rates separately for each of the domains and integrating (or averaging: see Materials and Methods) across all time points confirms this conclusion; k_C=–0.0066, –0.0065 and –0.0057 for the notochord, and left and right somite domains, respectively. Evidently, the rate of convergence is slightly higher in the notochord domain (~8% higher that the average of the somite domains in this example), a conclusion substantiated by similar estimates in a second wild-type embryo. Convergence in the notochord domain estimated by this method is in excellent agreement with that measured directly from its decreasing width with time (Fig. 4A; k_C=–0.0064 compared with –0.0066).

Kinetic analysis also confirms the relatively higher extension of the notochord domain when compared with the somite domain, noted above (Fig. 3D). Cells in the notochord domain have much higher AP velocities than somite domain cells beginning at the same AP position. The relationship between AP velocity and AP position, within either the notochord or somite domain, is linear (Fig. 4C). As we see from Fig. 4C, two separate lines describe the separate rates of extension of the two domains; the slope (k_E) is substantially higher for the notochord. Over all time points, extension in the notochord domain is about three times higher than in the somites in this embryo; k_E=+0.0064 for the notochord domain compared with +0.0023 for average of both somite domains.

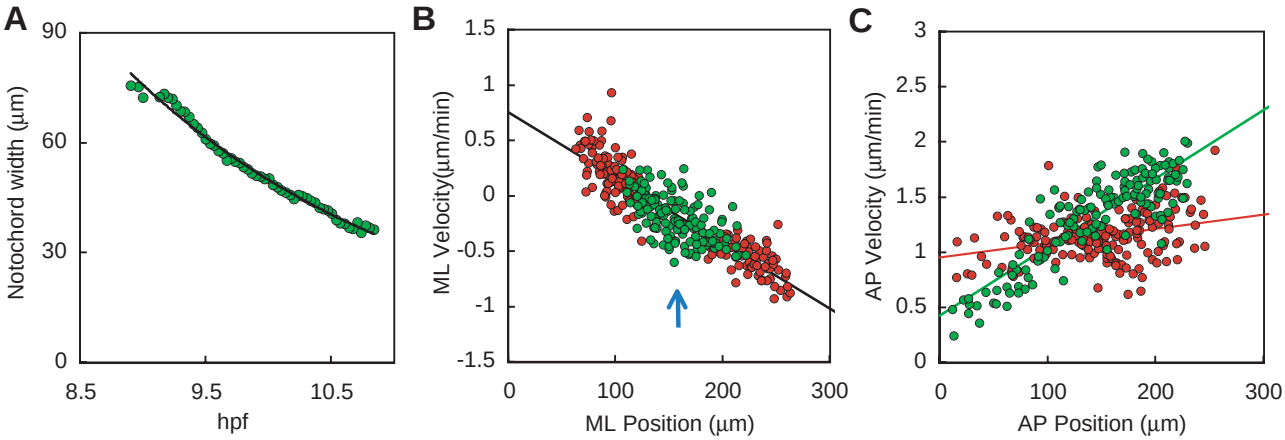

Fig. 4. Cellular kinetics during convergence and extension. (A) Kinetics of notochord domain convergence follows exponential decay. The rate of narrowing is represented by a single exponential fit to the data. The rate constant k_C is –0.0064. (B,C) Velocity versus position is linear for both convergence (B; k_C=–0.0059) and extension (C) (k_E=0.0062 for the notochord, green circles; k_E=0.0013 for the somite domain, red circles). The individual points represent velocities and locations of the entire field of tracked cells from one time sample, at 9 hpf (midgastrula stage). At this time point, k_C, is slightly lower than the value determined from the decreasing width of the field in A (–0.0059 min^{-1} versus –0.0064 min^{-1}). We observed that under the conditions of our recordings, k_C, measured as the slope of the gradient, is not stable time point to time point, rather the slope is 'jittery'. An 'average'/integrated estimate (see Materials and Methods) over the entire time period is –0.0073 min^{-1}, agreeing within 15% with the calculation from the notochord's change in width (A). The line of best fit was determined using linear regression. Gradients were assumed to fit when r^2 showed evidence for substantial explanation of variance and the F-statistic exceeded the P=0.05 significance threshold. The blue arrow in B indicates the position of the midline; here, the ML velocity is approximately zero.

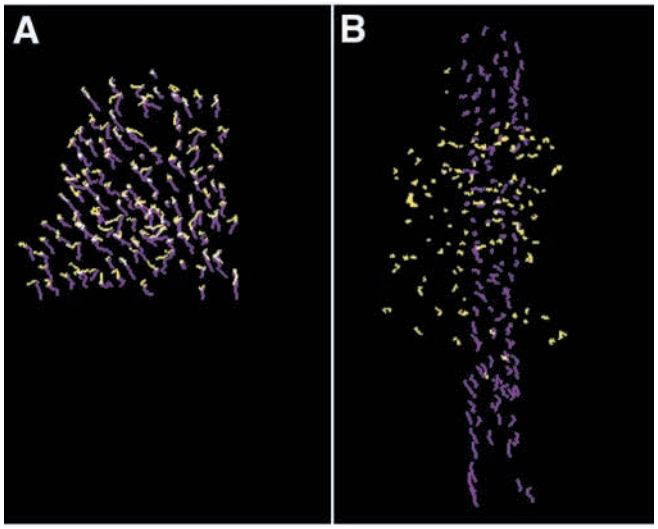

Fig. 5. MIB can account for all or most organized cellular movement within the wild-type notochord domain. Each purple line shows the observed movement pathway of individual cells over a 16 minute interval. The first 16 minutes of cell movement (A) and the last 16 minutes of cell movement (B, 4 hours later) of the recording used for Fig. 3 are shown. The yellow lines show the essentially random movements remaining after using the values of the convergent and extension rate constants to subtract the components of the cell movements due to MIB at every time point. At the beginning of the recording, before significant tissue shape changes have occurred (A), there is little difference between the location of the observed positions (purple) and the calculated positions with MIB removed (yellow). At the end of the 4 hour period, the observed field has undergone a significant shape change, convergence and extension (B, purple) but with MIB removed, the field has hardly changed shape at all. See Movie 6 at http://dev.biologists.org/supplemental/.

The rates of convergence and extension are expected to be equal if MIB is pushing cells apart exclusively along the AP axis (as in the model in Fig. 2) and if no factors, other than MIB, are contributing to convergence and extension. In this example, as predicted by this extreme model, convergence of the notochord domain almost exactly equals extension ($|k_C|$=0.0066 and $|k_E|$=0.0064; 3% difference). In a second wild-type embryo examined in this way, $|k_C|$ is 35% higher than $|k_E|$. By contrast, extension is much lower than predicted by the model in the somite domain, occurring, as we have seen at about one third of the predicted rate. An explanation that we favor for why convergence and extension are more in balance in the notochord domain than in the somite domain is that MIB is driving convergence at nearly the same rate in the two domains, but that during MIB, cells are rearranging themselves differently in the two domains (see Discussion).

The overall results of our kinetic analyses in wild-type embryos are in accordance with the MIB hypothesis. In particular, the kinetics of cell movement are approximately as predicted. Thus, MIB may account for all (or most) of the cellular movements within the wild-type notochord domain. To test this conclusion more rigorously, we ask if the velocity gradients underlying the cell movements, presumably generated by MIB, can account for the all observed convergence and extension of the notochord domain. We do

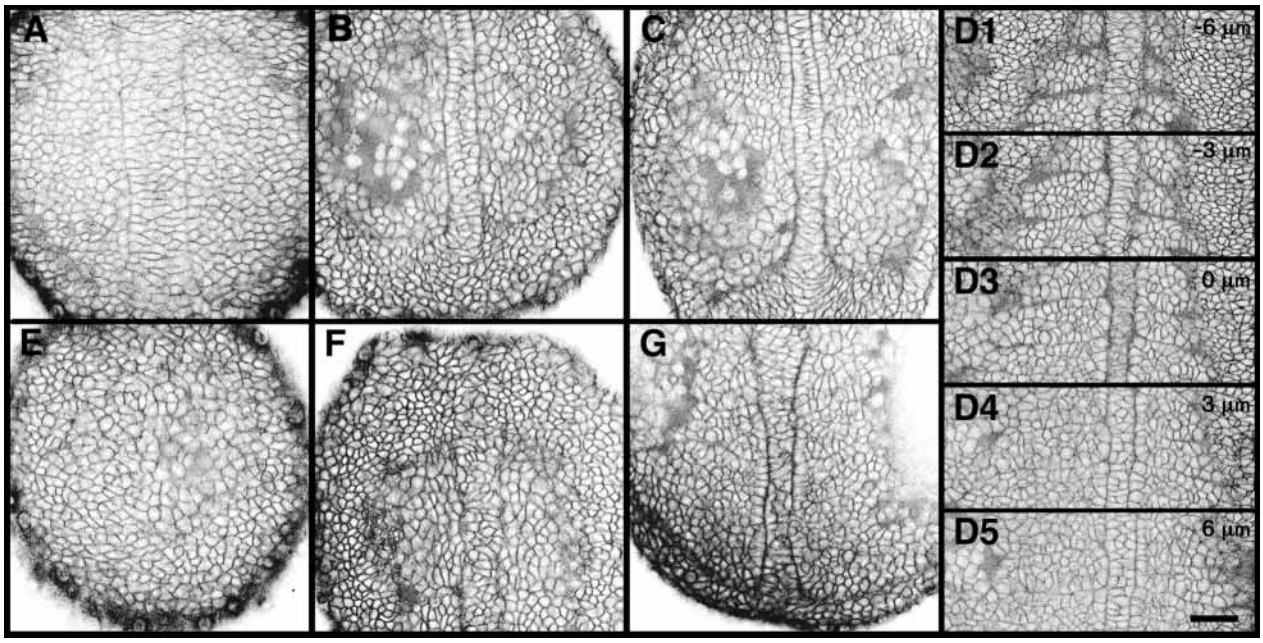

Fig. 6. Morphogenesis of the dorsal mesoderm is disrupted in the *no tail/Brachyury* mutant. Negative images of BODIPY-ceramide labeled preparations of wild type (A-C) and *ntl* mutants (E-G) at 9.5 (A,E), 10.2 (B,F) and 11 hpf (C,G). D1-5 show a through focus series (3 µm steps, shallow to deep) at the level of the second somite in another wild-type embryo at 11 hpf. D1 and D2 pass through the floor-plate region of the neural tube. D3 passes through the notochord-floor plate boundary. D4 and D5 pass through the notochord. In wild-type embryos, the notochord/somite boundary is apparent at 9.5 hpf (A), but in the *ntl* mutant a boundary between axial and paraxial domains begins to form only at 10.2 hpf (F). Cells become oriented along the ML axis, and exhibit a wedge-shape in the wild-type notochord-domain (B,C,D4,D5) but not in the mutant axial domain (E,F). Scale bar: 25 µm.

this by using the values of the convergence and extension rate constants to subtract the cell movement due to MIB. If MIB accounts for all cell movement, then this procedure should subtract all motion (other than random noise) from the field of cells. This is essentially what we observe, as illustrated for the notochord domain in Fig. 5. The purple lines indicate the observed locations and movements of the notochord cells at 7.3 hpf (Fig. 5A) and 4 hours later (Fig. 5B). Convergence and extension of the tissue are clearly observed. However, after removing the calculated components of the cell movements resulting from MIB, little convergence and extension is observed after 4 hours (yellow lines in Fig. 5). The field has approximately the same shape at the end as at the beginning. This analysis strongly suggests that we are not missing some major factor contributing to the change in shape of the field.

Failure of early convergence but not extension in the *no tail* mutant axial dorsal mesoderm

By the MIB model, active convergence drives extension in the dorsal mesoderm, and our analyses in the wild-type notochord and somite domains (see also below for cell neighbor analyses in the notochord) are consistent with this hypothesis. We reasoned that if convergence were abolished in the notochord domain, then so too should extension.

We used *ntl* mutants to carry out this experiment. The *ntl* gene encodes a T-box transcription factor (the zebrafish ortholog of mouse *Brachyury*) (Schulte-Merker et al., 1994) that is broadly expressed in nascent mesoderm and then maintained specifically in the gastrulating axial mesoderm that develops as notochord (Schulte-Merker et al., 1994). In *ntl* loss-of-function mutants, notochord development fails and gene expression analysis suggests that, within the *ntl*$^{-}$ axial domain, convergence fails during gastrulation (Melby et al., 1997).

Recordings made in the *ntl* mutant begin the same way as in the wild type. Cells ingress at the blastoderm margin in the early gastrula, and we made our recordings of the internalized dorsal mutant ‘mesodermal’ layer present during gastrulation. However, as gastrulation continues and the notochord-somite boundary becomes visible in the wild type, no such boundary is at first apparent in the mutant (Fig. 6A,E). Later, by the one-somite stage, a pair of boundaries appears in the mutant, encompassing an ‘axial’ domain only slighter broader than the wild-type notochord domain at this stage (Fig. 6B,F). We could use these boundaries in the mutant to score our tracked mesoderm-derived cells as ‘axial’ cells (i.e. cells enclosed by the boundaries) versus somitic cells (cells outside of the boundaries). The axial/somite boundaries appear not to enclose

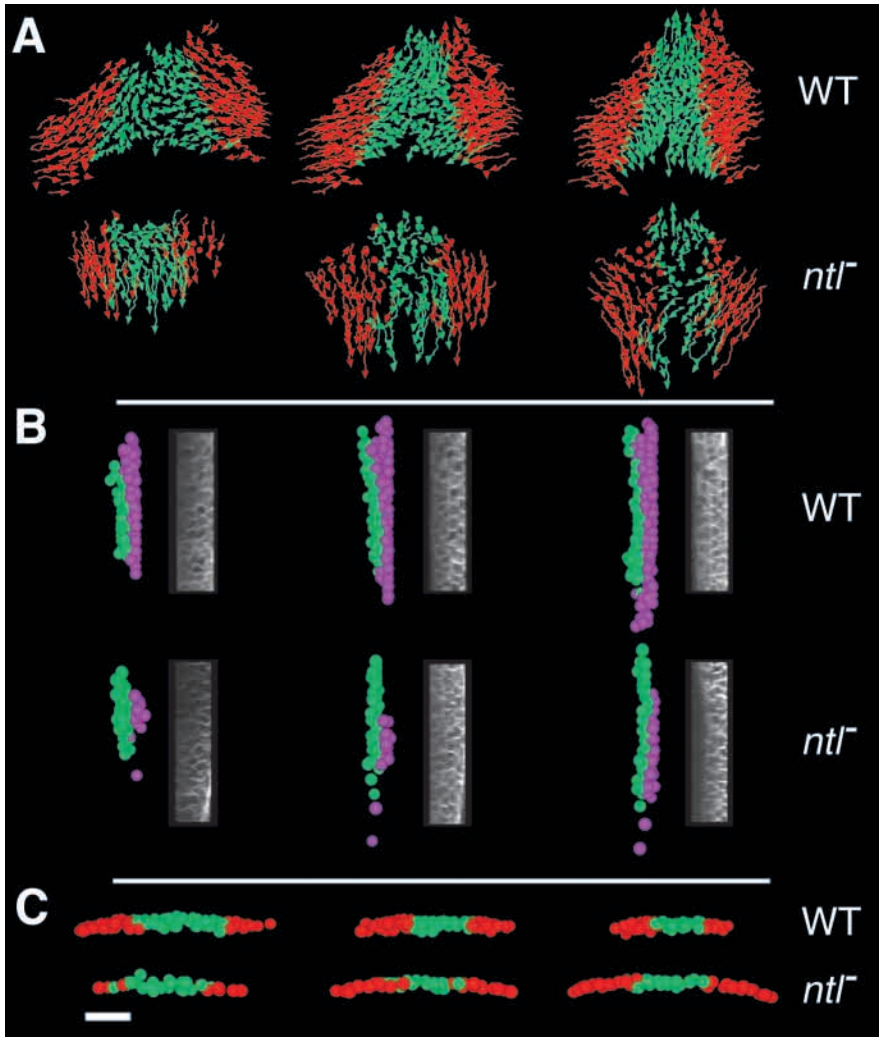

Fig. 7. Loss of function of *ntl* disrupts convergence but not extension. See Movies 7-12 at http://dev.biologists.org/supplemental/. The wild-type data are from the same 4D recording used for Fig. 4. Time points shown across A-C are 8, 8.8 and 9.5 hpf. (A) Cellular movement pathways in the notochord/axial (green) and somite domains (red). The arrows show the directions of cell movements and their lengths show the speed (the movement history during 16 minutes). Disruption of convergence (i.e. failure of the field to narrow) is evident in the *ntl*$^{-}$ axial domain: k_C for the axial domain in the mutant is –0.0017, when compared with –0.0073 for the wild-type notochord domain over the same time interval (8-9.5 hpf). Horizontally (ML) oriented tracks are largely missing in *ntl* mutant. However, extension, vertical lengthening of the field, is prominent in the mutant. (B) Intermixing does not occur between the notochord/axial domain (green) and the overlying midline epiblast (floorplate domain, magenta) in either the wild-type or *ntl* mutant (48 and 84 cells traced in wild-type and *ntl* epiblast, respectively). Side views made by 90° rotation of vertical strips of cells in the tracked data sets that are present at the dorsal midline at each time point. Accompanying these images, similar rotations from the original recorded BODIPY images reveal the boundary (Brachet’s cleft) between the two layers of cells in the wild type (notochord and floorplate), but this boundary is less apparent in the mutant. (C) The thickness of the region of tracked dorsal mesodermal cells does not change greatly during convergence and extension in the wild type, and may decrease slightly during extension without convergence in the *ntl* mutant axial domain (green). Scale bar: 50 μm.

a mutant notochord domain, however, but to enclose the ventral part of the primordium of the spinal cord (termed the neural keel at this stage) (Papan and Campos-Ortega, 1994). We infer this from the cellular morphology at early somite stages: in the wild-type notochord domain, the cells become highly organized. They take on a wedge-shape and are significantly elongated along the ML axis [Fig. 6C,D (parts 4 and 5)]. At a more dorsal focal plane in the wild type, just before coming to the floor plate one encounters the notochord-floor plate boundary, a flat, thin zone diffusely labeled with BODIPY-ceramide, where cell outlines are difficult to discern (Fig. 6D, part 3). Dorsal to this boundary the cells of the floor plate region are, at the three-somite stage, disorganized and irregular in shape (Fig. 6D, parts 1 and 2). In the *ntl* mutants at the same stage, the cellular morphology at any focal plane is irregular (Fig. 6F), like that of the wild-type floor plate. Furthermore, a notochord-floor plate boundary cannot be discerned.

The width of the axial domain in *ntl* mutants, as judged from the positions of the axial-somite boundaries, becomes very similar to that of the wild-type notochord domain, clearly revealing that the mutant axial domain has undergone convergence by the three-somite stage. In the wild-type embryo, as we have seen, the narrowing occurs during much of the gastrulation and early segmentation periods. By contrast, convergence of the axial domain in the *ntl* mutant is at first nearly absent. For example, the field of tracked mutant cells does not appreciably narrow during the 1.5 h interval during gastrulation shown as cell pathways in Fig. 7A, and by computed width of the field in Fig. 8A. Then, at postgastrula stages, just preceding the appearance of the boundaries surrounding the mutant axial domain, convergence of the mutant axial domain dramatically picks up (Fig. 8A; time points after about 9.5 hpf).

Notably, at same stages when convergence of the mutant axial field is severely perturbed, extension is occurring at a high rate. The field of tracked cells is lengthening quite prominently in Fig. 7A, and Fig. 8B shows that in this example, extension of the mutant axial domain is substantially higher than the wild-type notochord domain during the gastrula period. Without substantial convergence, seeing any extension at all during this period was unexpected. In the wild type, because of the close balance between convergence and extension, the cross-sectional (or planar) area of the notochord remains nearly unchanged (Fig. 8C; first a 20% increase then a 20% decrease over the recorded period). In the mutant, with marked extension but not convergence, the computed area of the domain expands markedly, about threefold, implying that an active process of extension or stretching is taking place (Fig. 8C).

A possible explanation for observing extension in the mutant comes from understanding that *ntl*$^{-}$ midline axial 'mesoderm' joins the ventral neural tube, and expresses the floor plate fate (Amacher et al., 2002; Halpern et al., 1993). We could suppose that, in the mutant, the mutant axial cells leave the axial mesodermal domain and move into the overlying epiblast-derived floor plate. These cells would then undergo rounds of cellular intercalation within the epiblast. Intercalations of axial mesodermal cells within the epiblast of *ntl* mutants may contribute to the observed extension of the axial domain. To examine this hypothesis, we tracked some epiblast cells overlying the midline axial domain in a *ntl* mutant. We observe

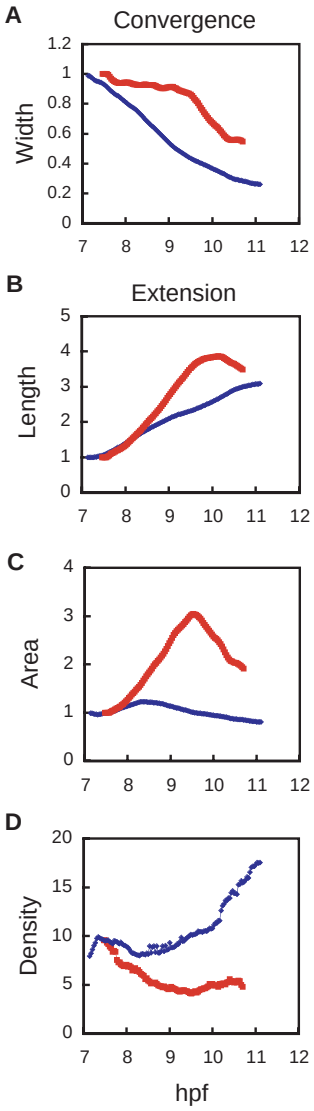

Fig. 8. Quantitative comparisons of features of morphogenesis of the wild-type notochord domain (blue) and the *ntl* mutant axial domain (red) during gastrulation and early segmentation stages. Values in A-C are normalized to 1.0 at the first time point. (A) Convergence: the domain widths are computed from values of k_C, estimated as in Fig. 3 at each time point (see Materials and Methods). Convergence is markedly decreased in the mutant until about 9.5 hpf. (B) Extension, domain lengths are computed from values of k_E, estimated as in Fig. 3 at each time point. In *ntl* mutants the axial domain extends rapidly during the same interval when the convergence is occurring slowly or not at all. (C) Area=width×length. The area is not expected to change if MIB alone underlies convergence and extension. Area only slightly decreases in the wild type, but increases in the mutant. (D) Cellular densities (number of cells per unit area). The density in wild type remains approximately constant during gastrulation and then increases. In the mutant, the density decreases, as would be expected if the field is increasing in area, extending but not converging.

that, as in the wild type, the two sets of cells do not mix (Fig. 7B). Hence, 'ectopic' intercalations between midline hypoblast and epiblast do not appear to account for the observed extension. Rather, during extension in the mutant, the cells seem to thin out, forming a layer one-cell thick (Fig. 7B,C). As the cells thin out, they cover a greater area, resulting in extension of the axial domain. The overall density of cells in the *ntl* mutant axial domain decreases, while the density of cells in the wild-type notochord increases (Fig. 8D). The observed decrease in cell density in *ntl* mutants also helps explain the increase in area, and extension, of the axial mesoderm (Fig. 8C).

MIB appears to initiate, but not to continue correctly in *no tail* mutant axial domain

Our analyses reveal cellular correlates of reduced convergence of *ntl* mutant axial domain cells during gastrulation. ML movements are present in wild-type embryos, but most sustained movements in mutants are AP (vertical versus horizontal tracks, Fig. 7A). In mutants, cells appear to mix abnormally between the axial domain and somite-forming

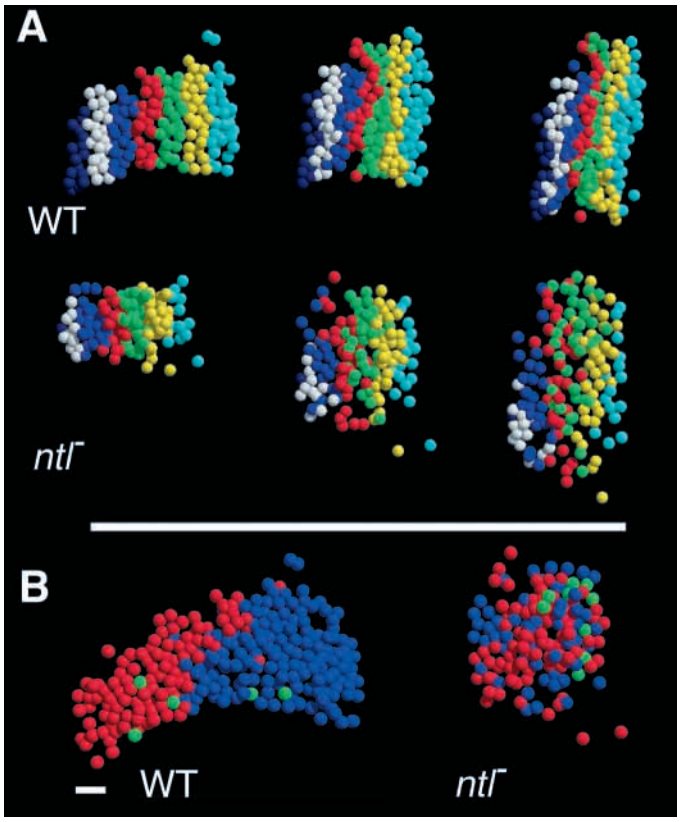

Fig. 9. (A) Extensive cellular mixing along the ML axis occurs in *ntl*$^{-}$, but not in wild-type embryos. Fields are shown at 8, 8.8 and 9.5 hpf, with the spheres representing tracked cells color-coded to produce vertical stripes (30 μm wide) at the first time (8 hpf). To facilitate comparison with *ntl*$^{-}$, only the medial portion (size matched with the *ntl*$^{-}$ field) of the tracked field is shown for the wild type. The stripes all narrow in the wild type and very little mixing is occurring between the stripes. In *ntl*$^{-}$, the stripes mix rather than narrow. (B) Cells move toward the midline in wild type, but move in a disorderly way with respect to the midline in *ntl*$^{-}$. Red and blue circles show cells moving to the right and left, respectively; green circles show cells with no left-right component to their movements at the representative time point illustrated (8.8 hpf). The center of each field corresponds the approximate midline for both A and B. See Movies 13-16 at http://dev.biologists.org/supplemental/.

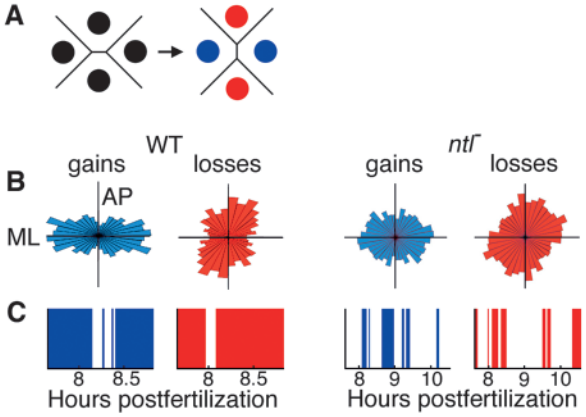

Fig. 10. Cells intercalate mediolaterally in both the wild-type and *ntl* mutant embryo (A,B), but only during brief intervals in the mutant, when compared with the wild type (C). (A) Intercalating cells become neighbors (blue, neighbor gains), pushing apart old neighbors (red, neighbor losses). Hence, for cells undergoing MIB, neighbor gains are ML (horizontal in the diagram) and neighbor losses AP (vertical; see also Fig. 2). (B) The polar plots show that these predicted behaviors are observed; the distributions are evidently broadened for the mutant. All four distributions are nonrandom (P<0.05; Watson's U^2_n test). The distributions are based on 623 gains and 633 losses for the wild type, and 1473 gains and 1822 losses for the mutant. (C) Colored bars show the durations of time periods when neighbor gains and losses are significantly oriented along any axis (Watson's test for nonrandom data). In the wild type, these periods of highly oriented activity are sustained during most of the time interval sampled. In the mutant, pulses of oriented and random behaviors are interspersed.

domains (Fig. 7A; red and green interspersed in *ntl*$^{-}$). Wild-type cells show only limited mixing with medial and lateral neighbors during convergence and extension (Fig. 9A). Of course, we expect limited mixing because constrained cell mixing is the basis of convergence and extension by MIB. However, ML mixing is prominent in *ntl* mutants (Fig. 9A), a circumstance where convergence is greatly reduced and mesoderm thins out. Cells in the wild type move towards the dorsal midline, as expected during MIB, but movement with respect to the midline is scrambled in *ntl* mutants (Fig. 9B).

These data show that the *ntl* mutant cells intermix far more extensively than do wild-type cells, but do not reveal how the intercalations are oriented. To address this, we examined cell neighbor exchanges. In cellular fields undergoing intercalations, new neighbor pairs will be generated and old ones lost in a reciprocal fashion. By the MIB model, neighbor gains should be oriented mediolaterally, and neighbor losses should be oriented anteroposteriorly (Fig. 2E,F; Fig. 10A). We detect large numbers of both neighbor gains and losses in the axial domains of wild-type and *ntl*$^{-}$ embryos, and in the wild type they are strongly oriented as predicted (Fig. 10B). Surprisingly, in *ntl* mutants, neighbor changes are still made with a significant but broadened tendency to align as in MIB (Fig. 10B). A most interesting change underlies the broadening. Analysis of the time course of the neighbor changing events (Fig. 10C) shows that the wild-type axial domain is able to maintain oriented intercalation activity nearly throughout the recording period. However, in the *ntl* mutant, only pulses of ordered neighbor gains or losses occur, interspersed with generally longer periods of disorganization.

This disorderly behavior suggests that MIB can be initiated but not sustained in *ntl* mutants, and prompted us to examine how cells are actually moving with respect to their local neighbors over both short and long time periods. We have shown that in a cellular field uniformly undergoing MIB, ML cell movement is towards the field center and AP movement is away from the field center, with velocity gradients accompanying both. If local cellular reorganizations are in fact uniform and if we now hold constant the position of any cell in the field, we expect ML neighbors to move towards that cell and AP neighbors to move away. Strikingly, we observe these predicted local correlates of both convergence and extension in the notochord domain of wild-type embryo (Fig. 11A). The ML inward movements are comparable in magnitude to the AP outward movements, reflecting the close balance of convergence and extension. Relative velocity gradients are evident (from the

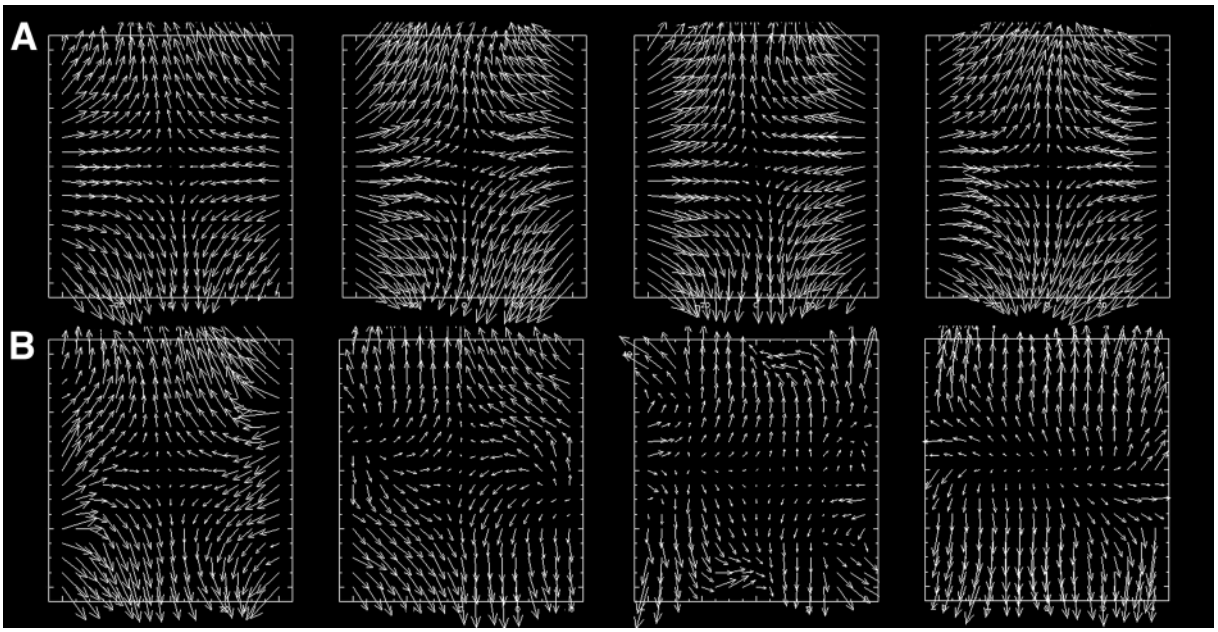

Fig. 11. Local cellular movement correlates of (A) convergence and extension in the wild-type embryo, and (B) of extension without convergence in the *ntl* mutant. The sets of panels show time sequences, at 4 minute intervals, for the notochord (WT)/axial (mutant) domains. For every cell in the field in turn ('reference cell', the point at the center of each plot), we calculate the displacements of all other notochord-domain cells relative to this reference cell, i.e. the cell movement toward or away from the reference cell. This is repeated for every cell in the notochord domain, each cell in turn taking the role of a reference cell. The data are then averaged for each time point, and the resulting averaged plots are shown. The arrows represent the average directions and speeds (length of arrow) of these relative movements; their placements on the grid are according to the positions of the cells relative to the reference cell. Inward cellular movements (i.e. horizontal arrows point towards the reference cell) correlate with convergence of the field, and outward movements (vertical arrows point away from the cell) correlate with extension. Inward movements are not sustained in the *ntl* mutant. Positions along the *x*-axis reflect positions along the AP axis relative to the reference cell while positions along the *y*-axis reflect positions along the ML axis relative to the reference cell. See Movies 17 and 18 at http://dev.biologists.org/supplemental/.

arrow lengths) along both axes, mirroring the global velocity gradients across the field. Furthermore, as shown by comparing the series of panels in Fig. 11A, the wild-type embryo is able to maintain these highly oriented local behaviors, i.e. the pattern is unchanging over significant time courses.

However, we see this same pattern only occasionally in the *ntl* mutant (Fig. 11B). Behavior is wild type-like at the first time point selected (first panel). Afterwards, whereas the AP movements tend to remain outward from the reference cell, the ML movements are scrambled, first inward (first panel), then outward (last panel in Fig. 11B). Disorganized local ML convergence of cells toward one another underlies the global disruption in convergence of the axial field.

DISCUSSION

Mediolateral intercalation behavior (MIB) may be the basic means by which dorsal mesoderm undergoes convergence and extension to establish the embryonic axis (AP axis) in any chordate (Keller et al., 2000; Munro and Odell, 2002a; Munro and Odell, 2002b). In this report, we have defined the global reshaping and local interactions we expect to see in a cellular field uniformly undergoing convergence and extension by MIB. We observe that both narrowing (convergence) and lengthening (extension) of the dorsal mesoderm occur as predicted by the MIB hypothesis. MIB is further strongly supported by our analyses of how local cellular neighborhoods are reorganizing during convergence and extension, and of the magnitudes and direction of movements of cells relative to their neighbors. The behaviors occur very uniformly across the entire notochord domain.

Our studies also reveal complexity in the behaviors that underlie convergence and extension. The notochord domain and adjacent domains of somite-forming cells converge at a similar rate, but they extend at different rates. In mutants that lack function of a key mesodermal patterning gene (the T-box gene *no tail*) (Schulte-Merker et al., 1994), convergence of the notochord domain is substantially blocked during gastrulation, but unexpectedly, the domain extends rapidly. A likely explanation for these findings, that we explore below, is that in addition to MIB, other morphogenetic force-generating processes are shaping the dorsal mesoderm during this crucial period of early development.

Mediolateral intercalation behavior quantitatively accounts for dorsal mesodermal convergence and extension

A striking finding of our study is that linear relationships, gradients, between cellular movement velocities and cellular position underlie both convergence and extension. These relationships arise because of the incremental and additive nature of ML intercalation events across the field: during convergence, cells located laterally will be displaced inward

towards the center of the field (the dorsal midline) not only by their own intercalations with their own neighbors, but because they are connected by a chain of adhesions to more medial cells, and cells all along the chain are undergoing MIB. The resulting velocity gradient along the chain will be linear, as we observed, if the local cellular behavior along the chain (i.e. MIB) is, on average, uniform. Exactly the same kind of explanation works to explain the AP gradient underlying extension.

These simple relationships between velocity and position are extremely useful in practice. If we plot cellular velocity versus cellular position, from our recordings of the cell movement pathways, the slopes of the lines are straightforward to determine. The slopes serve as rate constants (k_C, k_E) that reveal how rapidly the shape of the field is changing. It follows from the linear relationships that if MIB is constant over time, then the kinetics of the shape change are exponential (first order), as we confirmed experimentally.

From our estimate of k_C=–0.006 min^{-1}, halving of the width of the notochord domain occurs within 2 hours. The notochord domain is about 20 cells wide in the early gastrula (as determined from expression of the Not gene *floating head* at 6 hpf) (see Melby et al., 1996; Talbot et al., 1995). If the rate of convergence is constant, the domain will narrow to a domain only about a single cell wide during about 8 hours.

From our data, we propose that MIB is not only a prominent feature in dorsal mesoderm, but that this behavior quantitatively accounts for the shape changes of the field. We performed a severe test of this proposition for the notochord domain: From our measured velocities and locations of each cell in the field, we determined the overall values of k_C and k_E for the domain at each time point in our recording. Then, we computationally subtracted from the movement pathways of each cell those components (the ML and AP relocations) of the movements that were accounted for by the MIB. As predicted, the resulting movement pathways, with these components absent, exhibited no apparent trends. The cells jitter about in a possibly random fashion, and there was no prominent change in the shape of the field. Hence, MIB appears to be the single cellular morphogenetic behavior rearranging cells and shaping the dorsal mesoderm, during the mid- and late gastrula period. This finding is in marked contrast to descriptions of teleost dorsal mesodermal morphogenesis in literature from a century ago (e.g. Morgan, 1895). At that time, internalized dorsal mesodermal cells were proposed to migrate, with cell intercalations playing no role at all. By that model there would be no gradients, the migrating cells would all be moving with the same velocities. We observed mesodermal migrations without gradients on the ventral side of the zebrafish gastrula (data not shown) (Myers et al., 2002a). We observed no such cell migration in the dorsal trunk-forming mesoderm of the embryo.

Notochord and somite

We show that in the wild-type embryo, convergence of the notochord-forming mesoderm occurs at about the same rate as the adjacent somitic mesoderm. This finding suggests that during gastrulation, all of the trunk dorsal mesoderm is behaving as a single unit with respect to axis narrowing, i.e. there appears to be mechanical continuity across the entire field. This is an extremely interesting result because the field becomes subdivided during the same period by prominent notochord-somite boundaries. From cell lineage analyses we know that from the onset of gastrulation, within the dorsal mesoderm, the domain of prospective notochord cells is already a lineage compartment separate from the somitic domains (Kimmel and Warga, 1986; Melby et al., 1996). Our recordings also show that the domains are spatially separate during and after gastrulation: even as intercalations occur within the notochord and somite domains, they apparently do not occur across the notochord-somite boundaries, or between the two domains before the boundaries become recognizable. Moreover, by the stage our recordings begin, the notochord and somite domains are already expressing different patterns of developmental regulatory genes; genes encoding transcription factors, signaling molecules and adhesion molecules (Kodjabachian et al., 1999). Hence, it would be naive to imagine that the molecular basis of convergence of dorsal mesoderm is uniform.

Whereas the rates of convergence are similar for the notochord and somite domains, extension is much higher in the notochord domain, more than three times higher than in the somite for the wild-type example shown in Fig. 4C. If MIB is driving convergence at the same rate in both domains, then why are the rates of extension different? One possibility is that the cellular populations are rearranging differently during MIB. In the notochord, convergence and extension are in relatively close balance. We understand this to mean that essentially all of the ML intercalations are pushing cells apart along the AP axis, as in the model shown in Fig. 2. Hence the lengthening of the axis is proportional to its narrowing, and the area of the domain examined along the plane of the intercalations is preserved (Fig. 8A-C). However, in the wild-type somite domain, the intercalations might thicken the tissue as well as lengthen it; i.e. the ML intercalations would push some cells apart along the dorsoventral axis. Our data are consistent with this possibility (e.g. Fig. 7C), but our recording procedures were not optimized to quantify the thickening in the somitic domains. Whether the difference we observe is due to somitic thickening or something else, these findings reveal complexity of MIB, suggesting convergence and extension are separately regulated.

Conserved cellular basis of notochord convergence and extension

Mediolateral cell intercalations underlie convergence and extension of the notochord in *Xenopus* (Keller et al., 1989) in a way similar to what we observe in zebrafish. By midgastrula stages, the notochord-forming cells have a distinct bipolar shape and exhibit protrusive activities at their tips (Keller et al., 1989; Keller et al., 1992). Then they become wedge-shaped as the notochord narrows to a domain only one or two cells wide. During early morphogenesis, convergence of the *Xenopus* notochord is at least roughly balanced by extension (Keller et al., 1989). Convergence and extension also occurs in the somitic mesoderm in *Xenopus* (Keller et al., 2000). Extension is more rapid in the notochord, and shearing between the notochord and somite is observed. Intercalating somitic cells that do not contribute to extension may thicken the somites dorsoventrally (see Keller et al., 2000). Finally, disruption of the *no tail* ortholog in *Xenopus*, *Xbra*, disrupts convergence (Conlon and Smith, 1999).

In each of these features, the convergence and extension behavior and regulation appear similar in zebrafish and *Xenopus*, suggesting that the basic cellular machinery of MIB has been highly conserved between the two species.

One difference between zebrafish and *Xenopus* is that in zebrafish the yolk syncytial layer (YSL) provides a substrate for the mesendoderm, rather than a blastocoele roof present in amphibians. YSL nuclei undergo convergence and extension, and their movements are similar to those of the overlying mesendodermal cells (D'Amico and Cooper, 2001). This observation raises the possibility that the zebrafish cell movements are, at least in part, passively imposed by the YSL. However, passive convergence and extension of the zebrafish notochord-forming cells seem quite unlikely. Examined in detail, the blastoderm cell movements generally occur faster than the YSL nuclear movements (D'Amico and Cooper, 2001), arguing that convergence and extension are autonomous in the YSL and cellular blastoderm.

How might loss of *no tail* function disrupt convergence?

As expected from previous studies of gene expression of *ntl* mutants (Melby et al., 1997), we see a prominent defect in convergence of the gastrula-stage axial mesoderm – essentially the field does not narrow (Fig. 8A). The defect appears largely limited to the axial mesoderm and is transient, observed only during the gastrula period. Later, after epiboly is completed, convergence of the domain in the mutant begins at a rapid rate, and the domain width becomes similar to that of the WT notochord by the three-somite stage. It may not be coincidental that the time when convergence initiates in *ntl* mutants is when we see morphological boundaries enveloping the axial domain together with the ventral neural keel (including the floor plate) that undergoes pronounced convergence and extension. Notably, wild-type floor-plate cells do not express *ntl* at these stages: its axial expression is limited to the notochord. Hence, the *ntl*$^{-}$ cells, as they join the floor plate, may acquire the floor plate, *ntl*-independent, program of regulation of morphogenesis.

How does *ntl* regulate notochord morphogenesis, such that lack of function produces such a major defect? A candidate implicated in *Xenopus* is *Xwnt11* (Tada and Smith, 2001). This gene is a direct transcriptional target of the *ntl* ortholog *Xbra*. Dominant-negative constructs of *Xwnt11* (Tada and Smith, 2000), its receptor *Frizzled-8* (Wallingford et al., 2001b), or a key downstream target *Dishevelled/Xdsh* (Wallingford et al., 2000) all block convergence in *Xenopus*, apparently acting via a non-canonical planar polarity Wnt/Ca^{2+} pathway (Choi and Han, 2002; Tada and Concha, 2001; Wallingford et al., 2001a). Mutational analyses involving *silberblick/wnt11* (Heisenberg et al., 2000) clearly reveals a role in early morphogenesis of the *Xwnt11* ortholog in zebrafish. However, key aspects of Wnt11 regulation differ between the two species. *slb/wnt11* is first expressed in the early blastoderm margin, and this expression domain is independent of *ntl* (Makita et al., 1998). Midline *ntl*-dependent expression becomes strong only later, reaching highest levels at the 5- to 12-somite stages. Hence *slb/wnt11* is an unlikely candidate for mediating *ntl*-dependent MIB in the early axial mesoderm in zebrafish.

FGFs are attractive alternative candidates. FGFs are regulated by T-box genes, and are strongly implicated in the control of mesodermal morphogenesis, convergence and extension in particular. FGFs act via downstream targets including ephrins (Chong et al., 2000), and, like Wnt11, intracellular Ca^{2+} release (Nutt et al., 2001). Again there are key regulatory changes between *Xenopus* and zebrafish: in *Xenopus* the key *Xbra*-dependent FGF in axial mesoderm is eFGF, but in zebrafish other FGFs, including FGF8 and FGF3, play at least part of the role of this gene in dorsal mesodermal morphogenesis during gastrulation (B. Draper, personal communication).

Current understanding is that both noncanonical Wnt signaling and FGF signaling are regulating cell polarity as would be required for the cells to orient MIB properly. Interestingly, our analyses indicate that the major defect in *ntl* mutants may not be loss of cell polarity: We find that cells in the mutant can apparently initiate correctly oriented MIB. They frequently move towards their neighbors (Fig. 11), and make and break contacts with their neighbors (Fig. 10) in the same orientation as in the wild type. However, although many ML contacts are made in the mutant, the cells appear unable to exert the necessary tension to pull together – rather, they frequently slip apart. This proposal explains the ML cellular intermixing, as well as the randomized ML movement of cells with respect to the midline (Fig. 8) and one another (Fig. 11).

Loss of the tension necessary to pull the tissues together may reflect a requirement for an adhesion molecule missing in *ntl* mutants. Studies of the paraxially expressed T-box gene *spadetail* (*spt*; *tbx16* – Zebrafish Information Network) (Griffin et al., 1998) provide a clue about what might be missing from the *ntl*$^{-}$ convergence machinery. *spt* function is required for proper paraxial cell behaviors (Ho and Kane, 1990; Kimmel et al., 1989) and is hierarchically upstream of a protocadherin that is critical for proper mesodermal cell-cell adhesion during gastrulation (Kim et al., 1998; Yamamoto et al., 1998). Lack of a corresponding adhesion molecule in the *ntl*$^{-}$ axial domain (Kuroda et al., 2002) might underlie the defects we observe.

How can extension work when convergence does not?

Dorsal mesoderm efficiently extends in *ntl* mutants. It extends without significant convergence in the axial domain, clearly revealing that a mechanism other than MIB can drive extension in this domain. Furthermore, somitic mesoderm in the mutant also appears to extend more rapidly in the wild type, where, as discussed above, convergence normally seems to be driving thickening as well as extension.

The result comes as a surprise because there was no hint from our data, or from the literature, that anything other than MIB drives dorsal mesodermal extension. Finding that extension occurs in the mutant without convergence may well be providing a clue about how normal development works. For example, we do not understand what normally orients the AP pushing apart of cells during MIB such that convergence and extension are normally in balance in the notochord domain. The convergence-independent extension in the mutant may be uncovering something about this mechanism.

We examined specifically whether abnormal radial intercalation between axial hypoblast and epiblast might account for the observed extension in the mutant, and observed that it did not (Fig. 7B). However, radial intercalations are very likely to be occurring within (not between) these cell layers,

particularly in the dorsal mesoderm. We infer this because by late in gastrulation in *ntl* mutants (before convergence picks up in the mutant), both axial and paraxial mesoderm have thinned to a layer only a cell or two thick (Fig. 7C). During the same period, the cellular density of the mutant axial domain is substantially decreasing (Fig. 8D). Rather than packing together as in the wild-type notochord (which eventually becomes very cell-dense; Fig. 8D), the cells of the mutant axial domain are spreading apart predominantly in the AP direction, and this spreading accounts for the extension of the domain.

The cellular spreading observed in *ntl* mutants suggests that blastoderm epiboly could be driving extension in the mutant. Epiboly occurs simultaneously with convergence during the stages we studied. During epiboly, blastoderm cells intercalate radially (Kimmel and Law, 1985; Wilson et al., 1993) and spread apart along the AP axis (Concha and Adams, 1998; Warga and Kimmel, 1990). Solnica-Krezel et al. (Solnica-Krezel et al., 1996) previously suggested that epiboly contributes to extension in *volcano* mutants, and epiboly is underlain by an AP velocity gradient (R. J. A., D. Faruque and M. L. Concha, unpublished). We emphasize that our proposals for epiboly driving extension in the *ntl* mutant does not in any way argue against MIB as the key mechanism in the wild type. Indeed, in other mutants with disrupted convergence such as *knypek* and *trilobite*, or the *knypek-trilobite* double mutants, extension is also disrupted, even though epiboly is intact (Myers et al., 2002a). These genes function in the Wnt planar polarity pathway (Myers et al., 2002b) and the results, combined with our findings with *ntl*, might be revealing that Wnt signaling drives extension that is closely coupled to convergence, but that *ntl*$^{-}$ disrupts this relationship leaving other, parallel, mechanisms able to extend the axis. Furthermore, in epiboly mutants (Kane et al., 1996) or in embryos treated with a teratogen (Bauman and Sanders, 1984), both convergence and extension of the notochord can occur in the absence of epiboly, the opposite of the findings with the Wnt signaling mutants. Hence, it is likely that MIB normally functions redundantly with other cellular mechanisms to produce extension of the dorsal mesoderm. This proposition might be examined with new genetic analyses, e.g. in double mutants in which epiboly, Wnt signaling and *ntl* function are disrupted in combination. With the approach and quantitative methods we have developed for this study, we can now account for the individual reorganizations of populations of cells and distinguish between competing models for the mechanism of morphogenesis and its control.

We thank Charline Walker and Amy Biggs for technical assistance. Ray Keller, Peter B. Armstrong, Mark Cooper, Lilianna Solnica-Krezel, and members of the Institute of Neuroscience, University of Oregon, provided thoughtful comments on a draft of the paper. The research was supported by NIH grant HD22486 and an MRC Senior Research Fellowship to R. J. A.

REFERENCES

Amacher, S. L., Draper, B. D., Summers, B. and Kimmel, C. B. (2002). The zebrafish T-box genes *no tail* and *spadetail* are required for development of trunk and tail mesoderm and medial floor plate. *Development* **129**, 3311-3323.

Barber, C. B., Dobkin, D. P. and Huhdanpaa, H. T. (1996). The Quickhull algorithm for convex hulls. *ACM Trans. Math. Software* **22**, 469-483.

Bauman, M. and Sanders, K. (1984). Bipartite axiation follows incomplete epiboly in zebrafish embryos treated with chemical teratogens. *J. Exp. Zool.* **230**, 363-376.

Blagden, C., Currie, P., Ingham, P. and Hughes, S. (1997). Notochord induction of zebrafish slow muscle mediated by Sonic hedgehog. *Genes Dev.* **11**, 2163-2175.

Carmany-Rampey, A. and Schier, A. F. (2001). Single-cell internalization during zebrafish gastrulation. *Curr. Biol.* **11**, 1261-1265.

Choi, S. C. and Han, J. K. (2002). *Xenopus* Cdc42 regulates convergent extension movements during gastrulation through Wnt/Ca^{2+} signaling pathway. *Dev. Biol.* **244**, 342-357.

Chong, L. D., Park, E. K., Latimer, E., Friesel, R. and Daar, I. O. (2000). Fibroblast growth factor receptor-mediated rescue of x-ephrin B1-induced cell dissociation in *Xenopus* embryos. *Mol. Cell Biol.* **20**, 724-734.

Concha, M. L. and Adams, R. J. (1998). Oriented cell divisions and cellular morphogenesis in the zebrafish gastrula and neurula: a time-lapse analysis. *Development* **125**, 983-994.

Conlon, F. L. and Smith, J. C. (1999). Interference with brachyury function inhibits convergent extension, causes apoptosis, and reveals separate requirements in the FGF and activin signaling pathways. *Dev. Biol.* **213**, 85-100.

Cooper, M. S., D'Amico, L. A. and Henry, C. A. (1999a). Analyzing morphogenetic cell behaviors in vitally stained zebrafish embryos. *Meth. Mol. Biol.* **122**, 185-204.

Cooper, M. S., D'Amico, L. A. and Henry, C. A. (1999b). Confocal microscopic analysis of morphogenetic movements. *Methods Cell Biol* **59**, 179-204.

D'Amico, L. A. and Cooper, M. S. (2001). Morphogenetic domains in the yolk syncytial layer of axiating zebrafish embryos. *Dev. Dyn.* **222**, 611-624.

Devoto, S. H., Melancon, E., Eisen, J. S. and Westerfield, M. (1996). Identification of separate slow and fast muscle precursor cells in vivo, prior to somite formation. *Development* **122**, 3371-3380.

Essner, J. J., Laing, J. G., Beyer, E. C., Johnson, R. G. and Hackett, P. B., Jr (1996). Expression of zebrafish *connexin43.4* in the notochord and tail bud of wild-type and mutant *no tail* embryos. *Dev. Biol.* **177**, 449-462.

Griffin, K. J., Amacher, S. L., Kimmel, C. B. and Kimelman, D. (1998). Molecular identification of *spadetail*: regulation of zebrafish trunk and tail mesoderm formation by T-box genes. *Development* **125**, 3379-3388.

Hall, A. and Nobes, C. D. (2000). Rho GTPases: molecular switches that control the organization and dynamics of the actin cytoskeleton. *Philos. Trans. R. Soc. Lond. B Biol. Sci.* **355**, 965-970.

Halpern, M. E., Ho, R. K., Walker, C. and Kimmel, C. B. (1993). Induction of muscle pioneers and floor plate is distinguished by the zebrafish *no tail* mutation. *Cell* **75**, 99-111.

Heisenberg, C. P., Tada, M., Rauch, G. J., Saude, L., Concha, M. L., Geisler, R., Stemple, D. L., Smith, J. C. and Wilson, S. W. (2000). Silberblick/Wnt11 mediates convergent extension movements during zebrafish gastrulation. *Nature* **405**, 76-81.

Ho, R. K. and Kane, D. A. (1990). Cell-autonomous action of zebrafish *spt-1* mutation in specific mesodermal precursors. *Nature* **348**, 728-730.

Kane, D. A., Hammerschmidt, M., Mullins, M. C., Maischein, H. M., Brand, M., van Eeden, F. J. M., Furutani-Seiki, M., Granato, M., Haffter, P., Heisenberg, C. P. et al. (1996). The zebrafish epiboly mutants. *Development* **123**, 47-55.

Keller, R. and Winklbauer, R. (1992). Cellular basis of amphibian gastrulation. *Curr. Top. Dev. Biol.* **27**, 39-89.

Keller, R., Cooper, M. S., Danilchik, M., Tibbetts, P. and Wilson, P. A. (1989). Cell intercalation during notochord development in *Xenopus laevis*. *J. Exp. Zool.* **251**, 134-154.

Keller, R., Shih, J. and Domingo, C. (1992). The patterning and functioning of protrusive activity during convergence and extension of the *Xenopus* organizer. *Development Suppl.* 81-91.

Keller, R., Davidson, L., Edlund, A., Elul, T., Ezin, M., Shook, D. and Skoglund, P. (2000). Mechanisms of convergence and extension by cell intercalation. *Philos. Trans. R. Soc. Lond. B Biol. Sci.* **355**, 897-922.

Kim, S. H., Park, H. C., Yeo, S. Y., Hong, S. K., Choi, J. W., Kim, C. H., Weinstein, B. M. and Huh, T. L. (1998). Characterization of two *frizzled8* homologues expressed in the embryonic shield and prechordal plate of zebrafish embryos. *Mech. Dev.* **78**, 193-198.

Kimmel, C. B. and Law, R. D. (1985). Cell lineage of zebrafish blastomeres. III. Clonal analysis of the blastula and gastrula stages. *Dev. Biol.* **108**, 94-101.

Kimmel, C. B. and Warga, R. (1986). Tissue specific cell lineages originate in the gastrula of the zebrafish. *Science* **231**, 365-368.

Kimmel, C. B., Kane, D. A., Walker, C., Warga, R. M. and Rothman, M. B. (1989). A mutation that changes cell movement and cell fate in the zebrafish embryo. *Nature* **337**, 358-362.

Kimmel, C. B., Warga, R. M. and Kane, D. A. (1994). Cell cycles, clonal strings, and the origin of the zebrafish central nervous system. *Development* **120**, 265-276.

Kimmel, C. B., Ballard, W. W., Kimmel, S. R., Ullmann, B. and Schilling, T. F. (1995). Stages of embryonic development of the zebrafish. *Dev. Dyn.* **203**, 253-310.

Kodjabachian, L., Dawid, I. B. and Toyama, R. (1999). Gastrulation in zebrafish: what mutants teach us. *Dev. Biol.* **213**, 231-245.

Kuroda, H., Inui, M., Sugimoto, K., Hayata, T. and Asashima, M. (2002). Axial protocadherin is a mediator of prenotochord cell sorting in *Xenopus*. *Dev. Biol.* **244**, 267-277.

Makita, R., Mizuno, T., Koshida, S., Kuroiwa, A. and Takeda, H. (1998). Zebrafish wnt11: pattern and regulation of the expression by the yolk cell and No tail activity. *Mech. Dev.* **71**, 165-176.

Melby, A., Kimelman, D. and Kimmel, C. (1997). Spatial regulation of *floating head* expression in the developing notochord. *Dev. Dyn.* **209**, 156-165.

Melby, A. E., Warga, R. M. and Kimmel, C. B. (1996). Specification of cell fates at the dorsal margin of the zebrafish gastrula. *Development* **122**, 2225-2237.

Montell, D. J. (1999). The genetics of cell migration in *Drosophila melanogaster* and Caenorhabditis elegans development. *Development* **126**, 3035-3046.

Morgan, T. H. (1895). The formation of the fish embryo. *J. Morphol.* **10**, 419-472.

Munro, E. M. and Odell, G. (2002a). Morphogenetic pattern formation during ascidian notochord formation is regulative and highly robust. *Development* **129**, 1-12.

Munro, E. M. and Odell, G. M. (2002b). Polarized basolateral cell motility underlies invagination and convergent extension of the ascidian notochord. *Development* **129**, 13-24.

Myers, D. C., Sepich, D. S. and Solnica-Krezel, L. (2002a). Bmp activity gradient regulates convergent extension during zebrafish gastrulation. *Dev. Biol.* **243**, 81-98.

Myers, D. C., Sepich, D. S. and Solnica-Krezel, L. (2002b). Convergence and extension in vertebrate gastrulae: cell movements according to or in search of identity? *Trends Genet.* **18**, 433-488.

Nutt, S. L., Dingwell, K. S., Holt, C. E. and Amaya, E. (2001). *Xenopus* Sprouty2 inhibits FGF-mediated gastrulation movements but does not affect mesoderm induction and patterning. *Genes Dev.* **15**, 1152-1166.

Papan, C. and Campos-Ortega, J. A. (1994). On the formation of the neural keel and neural tube in the zebrafish *Danio (Brachydanio) rerio*. *Dev. Biol.* **203**, 178-186.

Schulte-Merker, S., van Eeden, S. F., Halpern, M. E., Kimmel, C. B. and Nüsslein-Volhard, C. (1994). *no tail* (*ntl*) is the zebrafish homologue of the mouse T (Brachyury) gene. *Development* **120**, 1009-1015.

Shih, J. and Keller, R. (1992a). Cell motility driving mediolateral intercalation in explants of *Xenopus laevis*. *Development* **116**, 901-914.

Shih, J. and Keller, R. (1992b). Patterns of cell motility in the organizer and dorsal mesoderm of *Xenopus laevis*. *Development* **116**, 915-930.

Smith, J. C., Conlon, F. L., Saka, Y. and Tada, M. (2000). Xwnt11 and the regulation of gastrulation in *Xenopus*. *Philos. Trans. R. Soc. Lond. B Biol. Sci.* **355**, 923-930.

Solnica-Krezel, L. (1999). Pattern formation in zebrafish–fruitful liaisons between embryology and genetics. *Curr. Top. Dev. Biol.* **41**, 1-35.

Solnica-Krezel, L., Stemple, D. L., Mountcastle-Shah, E., Rangini, Z., Neuhauss, S. C. F., Malicki, J., Schier, A. F., Stainier, D. Y. R., Zwartkruis, F., Abdelilah, S. et al. (1996). Mutations affecting cell fates and cellular rearrangements during gastrulation in zebrafish. *Development* **123**, 67-80.

Tada, M. and Concha, M. L. (2001). Vertebrate gastrulation: calcium waves orchestrate cell movements. *Curr. Biol.* **11**, R470-R472.

Tada, M. and Smith, J. C. (2000). Xwnt11 is a target of *Xenopus* Brachyury: regulation of gastrulation movements via Dishevelled, but not through the canonical Wnt pathway. *Development* **127**, 2227-2238.

Tada, M. and Smith, J. C. (2001). T-targets: clues to understanding the functions of T-box proteins. *Dev. Growth Differ.* **43**, 1-11.

Talbot, W. S., Trevarrow, B., Halpern, M. E., Melby, A. E., Farr, G., Postlethwait, J. H., Jowett, T., Kimmel, C. B. and Kimelman, D. (1995). A homeobox gene essential for zebrafish notochord development. *Nature* **378**, 150-157.

Wallingford, J. B. and Harland, R. M. (2001). *Xenopus* Dishevelled signaling regulates both neural and mesodermal convergent extension: parallel forces elongating the body axis. *Development* **128**, 2581-2592.

Wallingford, J. B., Rowning, B. A., Vogeli, K. M., Rothbacher, U., Fraser, S. E. and Harland, R. M. (2000). Dishevelled controls cell polarity during *Xenopus* gastrulation. *Nature* **405**, 81-85.

Wallingford, J. B., Ewald, A. J., Harland, R. M. and Fraser, S. E. (2001a). Calcium signaling during convergent extension in *Xenopus*. *Curr Biol* **11**, 652-661.

Wallingford, J. B., Vogeli, K. M. and Harland, R. M. (2001b). Regulation of convergent extension in *Xenopus* by Wnt5a and Frizzled-8 is independent of the canonical Wnt pathway. *Int. J. Dev. Biol.* **45**, 225-227.

Warga, R. M. and Kimmel, C. B. (1990). Cell movements during epiboly and gastrulation in zebrafish. *Development* **108**, 569-580.

Westerfield, M. (1995). *The Zebrafish Book: A Guide for the Laboratory Use of Zebrafish (*Danio rerio*)*. Eugene: University of Oregon Press.

Wilson, E. T., Helde, K. A. and Grunwald, D. J. (1993). Something's fishy here – rethinking cell movements and cell fate in the zebrafish embryo. *Trends Genet.* **9**, 348-352.

Yamamoto, A., Amacher, S. L., Kim, S. H., Geissert, D., Kimmel, C. B. and de Robertis, E. M. (1998). Zebrafish paraxial protocadherin is a downstream target of *spadetail* involved in morphogenesis of gastrula mesoderm. *Development* **125**, 3389-3397.

Zalik, S. E., Lewandowski, E., Kam, Z. and Geiger, B. (1999). Cell adhesion and the actin cytoskeleton of the enveloping layer in the zebrafish embryo during epiboly. *Biochem. Cell Biol.* **77**, 527-542.